



Potential impacts of mining of super-thick coal seam on the local environment in arid Eastern Junggar coalfield, Xinjiang region, China

Qiang Zeng^{1,2,3} · Li Shen^{1,2,3} · Jie Yang^{1,2,3}

Received: 26 June 2019 / Accepted: 2 January 2020 / Published online: 12 February 2020
© Springer-Verlag GmbH Germany, part of Springer Nature 2020

Abstract

Coal mining has serious impacts on local environment, including damage to the land and soil by subsidence, damage to ground-water systems through the fracturing and subsiding of overlying rocks, contamination of surface waters with acid mine drainage, and pollution of the atmosphere by release of toxic gases. The damage to ground water and its consequent impacts on the regional environment is the core of research of the coal mining from the perspective of environment protection. The present paper focuses on the changes of surface vegetation coverage, the pollutants released from pit coal power plants, and the damages to the ground aquifers induced by mining activities in arid Eastern Junggar coalfield of China. At first, the authors investigated the changes of surface vegetation coverage, since mining began in the 2000s using Landsat data. Results show that the low surface vegetation coverage (grade 1 plus grade 2) in the southern part of the region decreased from $11.62 \times 10^8 \text{ m}^2$ in 2003 to $9.57 \times 10^8 \text{ m}^2$ in 2017 (−17.6%), while it increased from $11.58 \times 10^8 \text{ m}^2$ in 2003 to $12.70 \times 10^8 \text{ m}^2$ in 2017 (+9.7%) in the eastern part. The high surface vegetation coverage (grade 3 plus grade 4) in the southern part increased from $1.94 \times 10^8 \text{ m}^2$ in 2003 to $4.00 \times 10^8 \text{ m}^2$ in 2017 (+106.2%), while it decreased from $4.39 \times 10^8 \text{ m}^2$ in 2003 to $3.26 \times 10^8 \text{ m}^2$ in 2017 (−25.74%) in the eastern part. The data of annual precipitation during the same period in this area show that the changes of surface vegetation coverage have less relationship with the annual precipitation, which indicates that the mining activities is probably the major factor for that. Second, a statistic of air pollutants generated from pit coal power plants was made based on data of references. Results show that the estimated gaseous pollutant emissions increased as 865.23 tons of smoke particles, 5940.73 tons of SO_2 , and 7584.48 tons of NO_2 in 2013, which increased rapidly with 9.73 times the smoke particle, 21.69 times the SO_2 , and 9.24 times the NO_2 than that of 2007. And then, the physical and numerical simulation of the damage of mining activities to aquifers was made to show the permeability of the reference points of overlying aquifers varies associated with mining activities. Results show that the porous rock matrix permeability has a negative relationship with fluctuation during mining, while the fracture permeability shows a positive one. Finally, a case investigation in southern area surrounding this coalfield was illustrated. Result shows that the local ground-water level decreased by 16 m difference from the altitude level of +774 m in 2003 to +758 m in 2013. Data and results from this study presented the already and the potential pollutions and damages to local environment induced by the mining activities in this region.

Keywords Eastern Junggar coalfield · Super-thick coal seam mining · Landsat data · Ground-water level · Numerical simulation

Introduction

The Eastern Junggar coalfield is located in the northern part of the Xinjiang region of China and named due to its proximity to the Junggar Basin. A park preserving dinosaur remains from the Jurassic period and the Caramali Nature Reserve are also situated in the northern part of this region. Surrounding this coalfield, especially in the south are the Qitai, Jimusar, and Mulei oasis areas where millions of people reside. These three oasis areas constitute the key farming

✉ Qiang Zeng
zengqiang@xju.edu.cn

¹ School of Resource and Environment Sciences, Xinjiang University, Urumqi 830046, China

² Institute for Arid Ecology and Environment, Xinjiang University, Urumqi 830046, China

³ Key Laboratory of Oasis Ecology of Ministry of Education, Xinjiang University, Urumqi 830046, China

zone of the Xinjiang region of China. Besides these natural conditions, the Eastern Junggar region is also well known for massive coal reserves, characterised by super-thick coal seam depositions. It is reported that the area of this coalfield is approximately 15,334 km² with a length of 200 km from west to east. After 2000, this coalfield was exploited and planned as a key centre of coal production for electricity and chemistry industries depending on it. More than 20 coal mines, including ground and surface mines, have been constructed since that time. Due to the aridness of the region (a fragile environment with less precipitation, little surface vegetation, thin layer of nutrient surface soil, etc.), some environmental problems, such as air pollution, disturbance and contamination of the soil, damage, and contamination of ground water, have emerged as serious issues associated with the mining of coal in this region. These problems will be ruinous without a good strategy to control them.

Numerous researchers have conducted studies on different aspects of the effects of coal mining. When assessing damage to land surfaces and soil caused by mining, there are two types of mining impacts to consider, i.e., the stripping of the land surface at open-cut sites and surface subsidence at ground coal mines. Both will bring consequent damage to surface vegetation. Liu et al. (2016) investigated the vegetation coverage of dumps in open-pit coal mine using Landsat data from 1990 to 2015. Results showed that water level greatly influenced the growth and development of vegetation; there was greater vegetation coverage at high elevation and less coverage on steep slopes. Huang et al. (2015, 2016) investigated the vegetative succession soil infiltration characteristics of five different restoration models at refuse dumps. A multiple linear regression analysis indicated that the infiltration rate was primarily determined by the silt percentage, soil organic matter (SOM), plant coverage, and the variation in soil bulk density. The changes in plant species diversity and succession of soil physicochemical properties in re-vegetated refuse dumps of varying ages suggest that soil and vegetation recovery are equally important in eco-restoration activities in semiarid areas. Yongjun et al. (2018) investigated the vegetation patterns and responses to underground mining using remote-sensing data. Results demonstrated that hydrological factors and soil attributes, including groundwater levels, soil organic matter, and soil moisture, control the structure of the local vegetation community. Silva et al. (2018) investigated the impact of greenhouse gases produced from surface coal mining in Brazil. Daozhong et al. (2011) conducted a comparative analysis of ecological pressures between open-cut and underground coal mining, using the method of ecological burden. Their result showed that the total ecological burden and the coefficient of ecological burden of open pit are 4.31–11.36 times and 2.77–7.74 times than that of underground coal mines,

respectively. Underground coal mining is recommended if there is a choice between the two mining methods. Huertas et al. (2012) studied and established models demonstrating the total suspended particulates (TSP) and PM₁₀ dispersion occurring around open-cut coal mines in Columbia, based on collection of topographic and meteorological information for the region. Reisen et al. (2017) investigated the emission of harmful substances produced by coal combustion at an open-cut coal mine in Australia. Results showed that the air pollution was considerable during coal combustion at this site. Espitia-Pérez et al. (2018) investigated the contribution of particulates to cytogenetic damage in residents living near an open-pit coal mine. Results indicated that there was a spatial relationship between exposure to elevated concentrations of PM_{2.5} and PM₁₀, and micronuclei frequency in bi-nucleated and mono-nucleated cells. Reclamation of coal mine area also is one important aspect of mining-related eco-environmental issue research. Kumari and Maiti (2019) investigated the change of carbon and nitrogen pool accretion during reclamation using grass and legume. Results show that the legume has much more advantage over the grass species to restore the coal mine soil fertility.

Concerning the damage and contamination to ground water, the damage to overlying aquifers is an area of focus. This damage will bring about regional redistribution of surface and subsurface water. This redistribution leads to a change in surface vegetation coverage. Zhao et al. (2017) analysed the impact of surface coal mining on ground water using Modflow tool. Results showed that water from aquifers present a potential risk for mining operations in surface open-cut coal mine. Bahrami et al. (2016) predicted the groundwater inflow into an advancing open-pit mine and the hydraulic head in observation wells at different distances from the centre of the pit during its advance, using the Artificial Neural Network hybrid models. Huisamen and Wolkersdorfer (2016) proposed a method for the geochemical modelling of transient contaminant release from rehabilitated opencast coal mines. Simulation from this model using groundwater monitoring data demonstrated the hydro-geochemical evolution of mine water over time. Hussain et al. (2019) investigated the effects of coal mining on the quality of surface water and groundwater in the Handan region in China. Result showed that the spatial distribution of chemical constituents declines with the distance from mining areas. And the elemental enriched coal-rock has caused the pollution of groundwater by rock weathering and percolation.

In this paper, the authors seek to quantify the impacts of mining of the super-thick coal seam on local environment in the Eastern Junggar coalfield, one of the biggest coalfields around the world, by investigating the disturbance to surface vegetation coverage, the air pollution induced by pit power plants, as well as the damage to ground aquifers, etc.

Study area

The Eastern Junggar coalfield is in the eastern part of Junggar terrain. It orients from west to east, with a length of about 200 km, and it occupies an area of approximately 15,334 km². Since 2000, several companies have invested in the construction of coal mines in this coalfield, which was divided into four mining areas from west to east: the Wucaiwan mining area, the Dajing mining area, the Jiangjunmiao mining area, and the Xiheishan mining area (Fig. 1).

The coal-accumulating basin was formed as a skirt-edge structure with a series of nose-form anticlines and dustpan-form synclines, which were named the Shuangjin-gzi–Jiangjunmiao anticline, the Bailitan anticline, the Xiheishan anticline, the Beishanyao syncline, and the Dongheishan syncline, from west to east in this region. There also are two faults, named the West Dongheishan fault and the East Dongheishan fault. In this region, most of the coalfield are a result of Quaternary, Neogene, Jurassic, and Carboniferous formations. There are deposits with more than one coal seams in the different depths of the

Jurassic formations. Amongst these coal seams, coal seam B is featured with the super-thickness up to 90 m, which is the major coal mining seam in this region (Fig. 2).

This coalfield is surrounded by rivers/streams in the southern, eastern, and northern parts of the region; all rivers/streams originate from the Tianshan and Altai Mountains. Some of these rivers are seasonal, while others are annual. It is well known that the main water resources in the Xinjiang region originate from the mountains, where precipitation and glacial water flow from high elevation areas to low elevation areas and onward to the centre of the basins. Figure 3 shows the surface water distribution in part of Qitai County situated in the southern part of the Eastern Junggar coalfield.

From Fig. 3b, it is sure that the mining of coal seam will have serious effects on the local environment due to the subsidence of overlying rocks and surface which will lead to the change of the path of surface and subsurface water flow.

Concerning the super-thickness of the coal seam in the Eastern Junggar coalfield, two traditional mining methods were employed to extract the coal, i.e., open-cut and underground mining methods (see Figs. 4 and 5). Currently, there are more than ten open-cut sites existing in this coalfield;

Fig. 1 Map of the Eastern Junggar coalfield

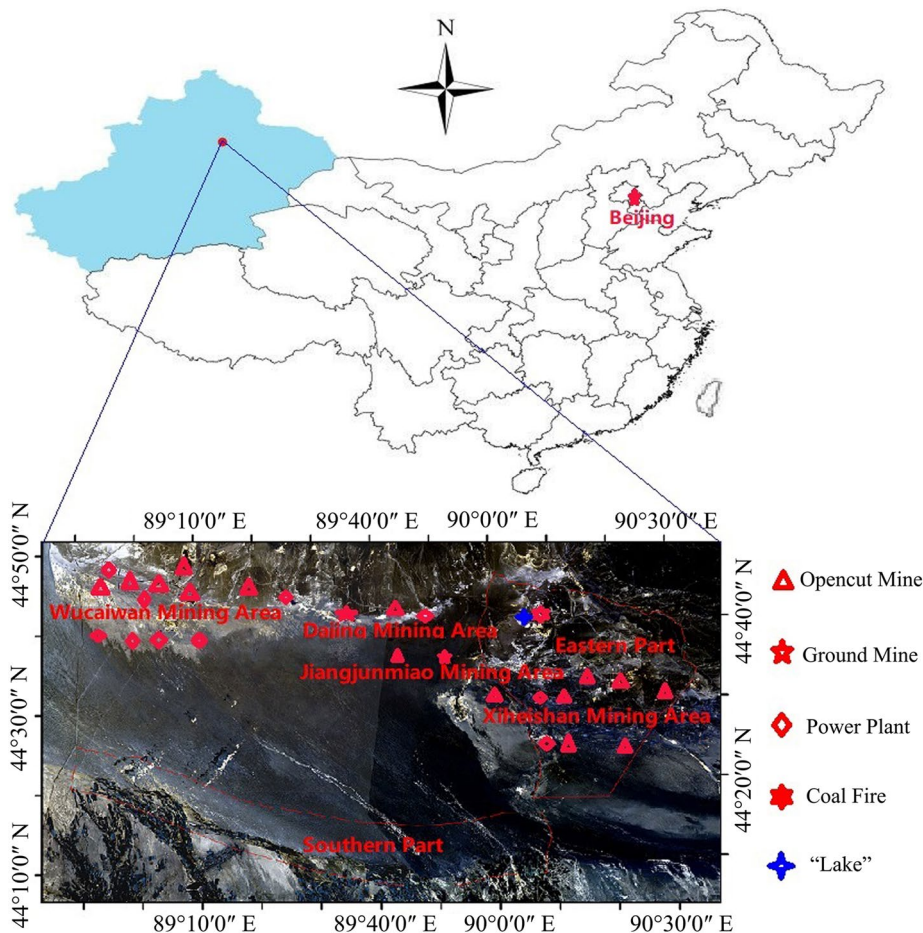


Fig. 2 Profile of coal seam B deposition in the Eastern Junggar coalfield

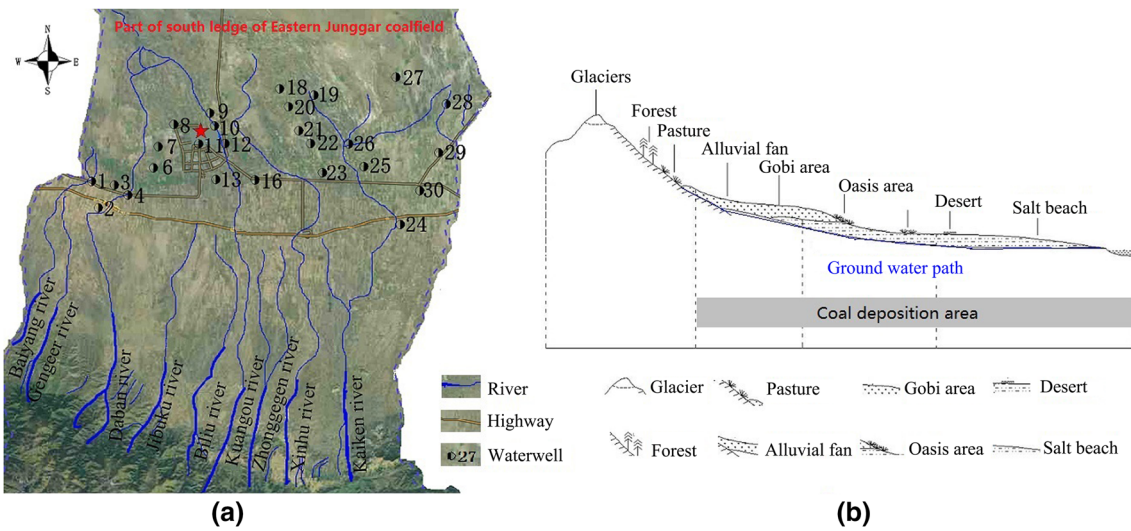
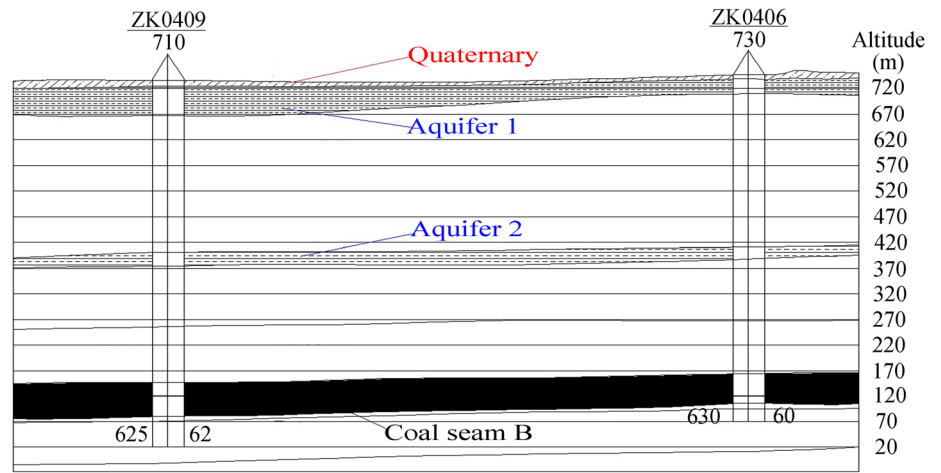


Fig. 3 Features of water sources in the Xinjiang region. **a** The distribution of rivers in southern part of this region. **b** The typical map of water routine from mountain to basin

Fig. 4 Open-cut mining of coal seams in the Wucaiwan mining area of the Eastern Junggar coalfield

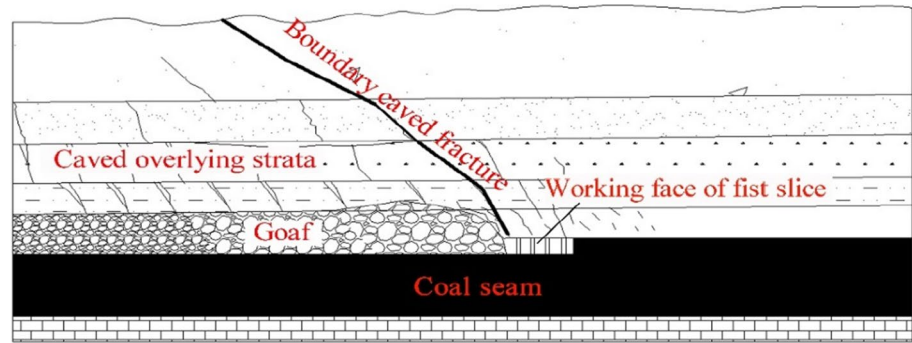


there are only two underground mines, in the Dajing and Jiangjunmiao mining areas.

In the open-cut mining of coal, there are generally three steps: the stripping of the surface layer of soil to reach the

coal seam, the digging of the coal seam to upload coal to the trucks, and the transportation of coal to surface stocking sites using trucks, etc. In this region, there are

Fig. 5 Schematic diagram of underground mining method



15 open-cut coal mines which were designed to produce 117.95 million tons of coal annually.

To conduct underground mining of the super-thick coal seam, shafts and underground tunnels need to be constructed to reach the coal seam and working face. According to field survey data, there are two underground coal mines in the Eastern Junggar coalfield, the No. 2 Colliery of State Grid (15 million tons of coal production annually) and the No. 1 Colliery of Xinjiang Lu'an Energy & Chemistry Co. Ltd (5 million tons of coal production annually), respectively. Due to the deposition of the coal seam and its thickness of up to 90 m, the long-wall top-caved mechanical slice mining method, which has a mining height of up to 7 m for each sub slice layer, will be employed in these two underground mines. The first level of mining is planned at the altitude of +500 m with a direct distance of 300 m to the surface. At present, all shafts and tunnels for the first level of mining for these two underground mines have already been constructed.

Changes of surface vegetation coverage

Surface vegetation coverage changes in the Eastern Junggar coalfield were investigated by inversing Landsat 8 images collected since 2003. To obtain relatively accurate image data, the images for the summers of 2003, 2004, 2006, 2009, 2011, 2013, 2016, and 2017 were downloaded from the USGS website. The quality of the images for the same period in the remaining years between 2003 and 2017 was not good enough to justify inversing that these images were not included in this study.

The vegetation coverage is generally obtained using a combination of the near-infrared, infrared, and other bands. In practice, the vegetation coverage index is typically used to describe the changes in surface vegetation, which is based on remote sensing. The normalised difference vegetation index (NDVI) was obtained from the ratio of the difference value and the total value of both the near-infrared and visible-infrared bands. This index can be calculated using the following equation:

$$\text{NDVI} = \frac{\text{NIR} - \text{Red}}{\text{NIR} + \text{Red}}, \quad (1)$$

where NDVI is the normalised different vegetation index, NIR denotes the value of the near-infrared light, and Red denotes the value of the visible infrared light. The ENVI 5.4 tool (Exelis VIS Co. Ltd., USA) is used to calculate the vegetation coverage:

$$P_V = \frac{\text{NDVI} - \text{NDVI}_s}{\text{NDVI}_V - \text{NDVI}_s}, \quad (2)$$

where P_V denotes the vegetation coverage (%), NDVI_V denotes the maximum NDVI, and NDVI_s denotes the minimum NDVI.

Based on the remote-sensing images from Landsat 8, Eqs. (1) and (2), and the application of ENVI tool, the changes of the surface vegetation coverage in the eastern and southern parts of the coalfield (2013–2017) were plotted (Figs. 6, 7).

To investigate the changes of surface vegetation, the extent of surface vegetation coverage in the eastern and southern parts of the Eastern Junggar coalfield were classified into four grades according to the coverage indicated by remote-sensing data: grade 1 was less than 10% vegetation coverage, grade 2 was 10–30% vegetation coverage, grade 3 was 30–70% vegetation coverage, and grade 4 was 70–100% vegetation coverage. The surface vegetation coverage statistics based on Figs. 6 and 7 are presented in Table 1. To help determine the reason for these vegetation coverage changes, the annual precipitation of the region was also determined (Table 1).

To compile the data for areas that had different grades over the years, the changes for each grade from 2003 to 2017 were plotted (see Figs. 8, 9).

From Fig. 6, it was observed that the distribution of grade 3 coverage in south area of the eastern part decreased from 2004 to 2017. From Fig. 7, it was illustrated that the distribution of different grade coverages changed in different area of the southern part of Eastern Junggar coalfield from 2003 to 2017 with fluctuations. From Fig. 8, it is obvious that the grade 4 coverage area stays at a stable level after 2004 in the

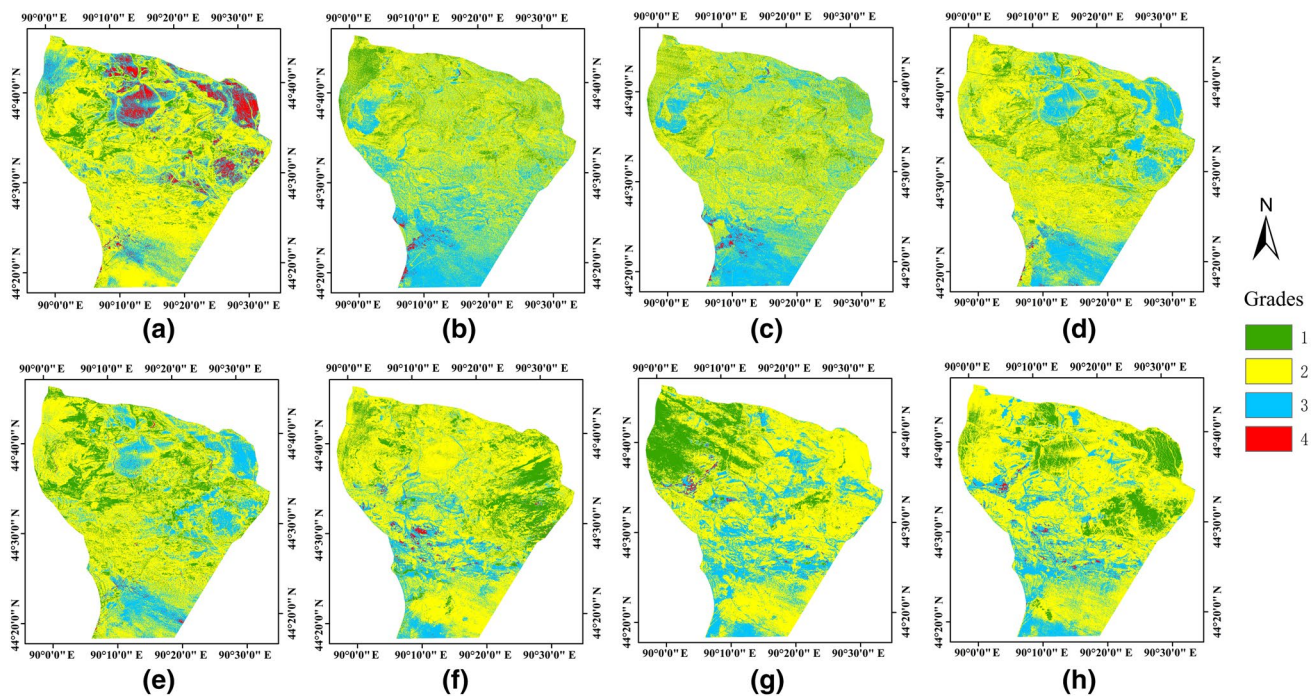


Fig. 6 Changes of surface vegetation coverage distribution in the eastern part of the Eastern Junggar coalfield [from 2003(a) to 2017 (h)]

eastern part of the Eastern Junggar coalfield, and Fig. 6b–g show the same trend of it. The areas of the grade 1 and grade 2 tended to increase from 2003 to 2017, while the area of grade 3 tended to decrease during the same period. In southern part of this coalfield (Fig. 9), it was also observed that the grade 3 and grade 4 areas tended to increase from 2003 to 2017. Conversely, the grade 1 and grade 2 tended to decrease during the same period.

The relationship between grades (the low grade of grade 1 plus grade 2 and high grade of grade 3 plus grade 4) of surface vegetation coverage and the precipitation also was investigated using data from Table 1, see Figs. 10 and 11.

From Figs. 10 and 11, it is obvious that the change of low surface vegetation coverage in both parts show an inverse trend of change. In eastern part, the low surface vegetation coverage has more close relationship with the precipitation than that of other grades and that of southern part. From this analysis, it is sure that the precipitation did not give an effect on changes of surface vegetation coverage which we expected. One possible reason for that is the mining activities' act on surface vegetation include the truck transportation, dust dissipation and settlement, and mining-induced surface subsidence and fracturing.

Besides the change in surface vegetation coverage, there are also some special landscapes that can be observed in this region, especially surface coal fires caused by mining. Due to the shallow deposition of this super-thick coal

seam, surface mining has also been conducted in past years, especially in the Jiangjungebi mining area of this coalfield. According to author's latest field campaign to surface mining, there exists a trench about 4 km long and 100 m wide in this area, mining of which has caused two coal fires named as the Jiangjungebi and Jiangjunmiao coal fires. Photograph taken by the author in July 2018 (Fig. 12) shows the presence of a "lake" in the west part of this trench depicting a special combined landscape of water and burnt coal. The "lake" is bordering to the burnt coal area with barriers of soil formed naturally. The reason for the existence of this "lake" might be the outflow of water from the subsurface aquifers that were damaged during the surface mining.

Estimation of typical pollutants

The public is mainly concerned about the pollutants generated from coal mining, including gases, solids, as well as liquid pollutants. The most common gaseous pollutants reported include: floating dust and harmful gases (such as CO, CO₂, and CH₄). It was reported that there are ten coal power plants (seven plants situated in Wucaiwan mining area, two plants situated in Xiheishan mining area, and one plant situated in Dajing mining area) in Eastern Junggar coalfield which generate electricity for supply to eastern China. Based on data collected from 2007 to 2013, the possible gaseous pollutant emissions increased from 84.7 tons

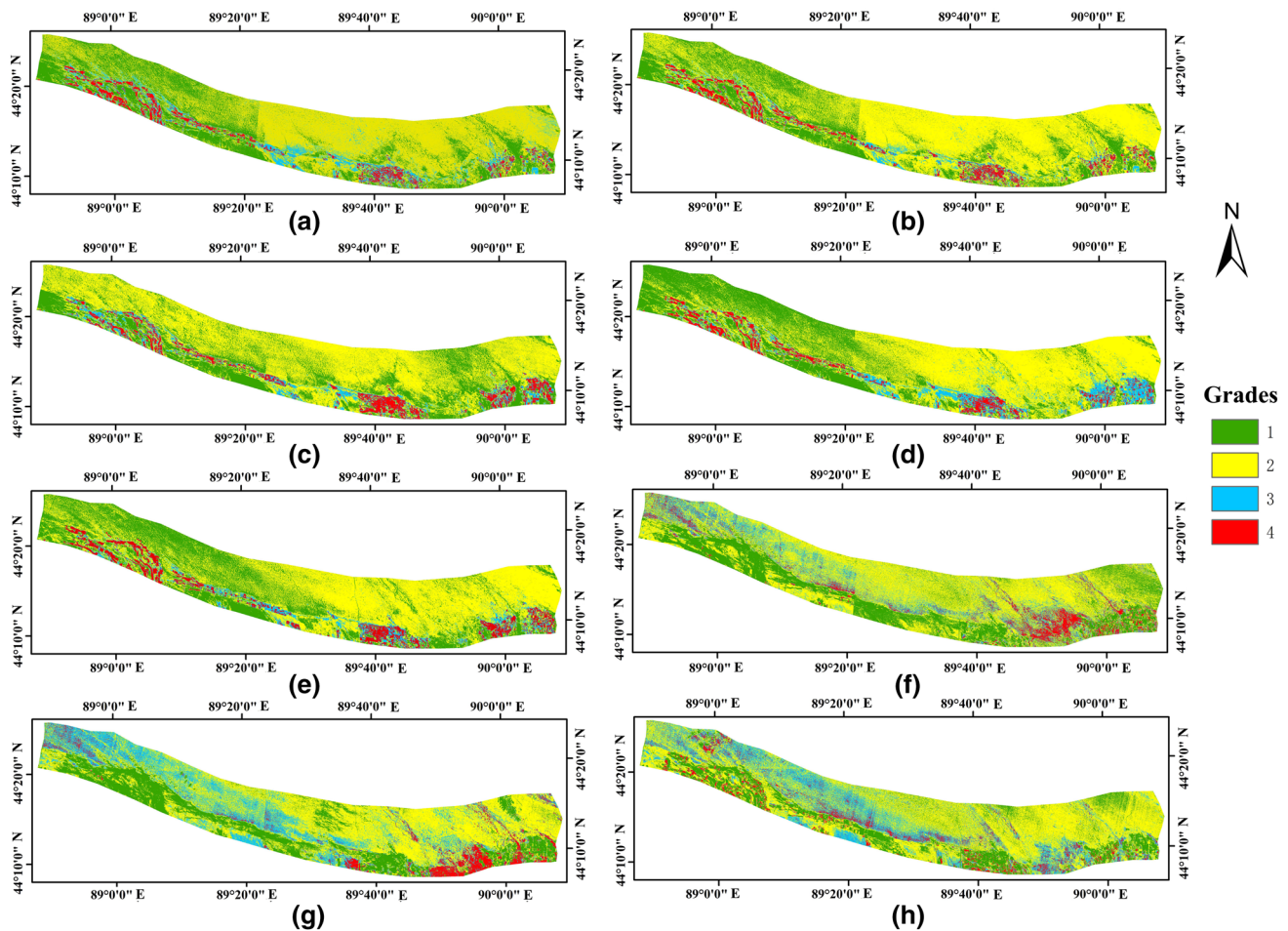


Fig. 7 Change of surface vegetation coverage distribution in the southern part of the Eastern Junggar coalfield [from 2003(a) to 2017 (h)]

of smoke particles, 273.8 tons of SO_2 , and 820 tons of NO_2 in 2007 to 865.23 tons of smoke particles, 5940.73 tons of SO_2 , and 7584.48 tons of NO_2 in 2013 (Table 2) (Jie 2015). The amount of these gaseous pollutant emissions increased rapidly, with about 9.73 times the smoke particle, 21.69 times the SO_2 , and 9.24 times the NO_2 .

Besides the gaseous emissions, other by-products of coal mining and coal power plants are also generated. The flying ash produced by coal power plants usually contains compounds such as SiO_2 , Al_2O_3 , FeO , Fe_2O_3 , CaO , TiO_2 , MgO , K_2O , Na_2O , SO_3 , and MnO_2 , which are detrimental to health. According to the number of pit coal power plants and the installed capacities in this region (Table 3) (Jie 2015), it was estimated that more than 1.9476 million tons of fly ash will be generated annually as a by-product of the generation of electricity, and approximately 7500 acres of land would be required for its storage. Some of the harmful components of fly ash can penetrate the subsurface by leaching of precipitation during storage, leading to possible contamination of ground water.

The dispersion range of pollution is mainly determined by local meteorological conditions. Concerning this aspect, the authors collected historical reports of local meteorological survey data, such as the dominant wind direction, the changes in the wind, and the precipitation, etc. The data showed that the dominant wind direction is always orientated east–south which means that the wind always originates from northeast to southeast. Concerning the distributions of surrounding towns and residential communities, there is certainly a risk that the gaseous pollutants and fly ash will be transported to the residential communities of Qitai, Jimusar, and Mulei Oasis, which could lead to local air pollution as well as soil and water contamination. Some of the particle pollutants could also be transported to the Tianshan Mountains where glaciers exist. It is well known that these glaciers are the main sources of water for people surviving in the arid region of Xinjiang. From this consideration, these gaseous pollutants and by-products of coal mining and coal power

Table 1 Vegetation cover in the vicinity of the study area from 2003 to 2017

Year	Areas with different vegetation coverage grades ($\times 10^8 \text{ m}^2$)						Precipitation (mm)
	1	2	1+2	3	4	3+4	
2003							
East	1.57	10.01	11.58	3.26	1.13	4.39	200.40
South	3.99	7.63	11.62	1.25	0.69	1.94	
2004							
East	1.89	8.96	10.85	5.02	0.08	6.00	249.50
South	3.89	8.08	11.97	0.80	0.78	1.58	
2006							
East	1.74	9.23	10.97	4.89	0.11	5.00	155.30
South	4.27	7.51	11.78	0.90	0.88	1.78	
2009							
East	2.03	10.03	12.06	3.86	0.04	3.90	198.90
South	4.21	7.24	11.45	1.37	0.74	2.11	
2011							
East	2.75	9.69	12.44	3.43	0.09	3.52	225.80
South	4.49	7.17	11.66	0.92	0.97	1.89	
2013							
East	2.52	10.69	13.21	2.59	0.15	2.74	219.50
South	3.54	6.83	10.37	2.14	1.06	3.20	
2016							
East	2.37	9.92	12.29	3.58	0.09	3.67	185.00
South	3.09	6.54	9.63	3.02	0.91	3.93	
2017							
East	2.19	10.51	12.70	3.15	0.11	3.26	45.70
South	2.62	6.95	9.57	3.02	0.98	4.00	

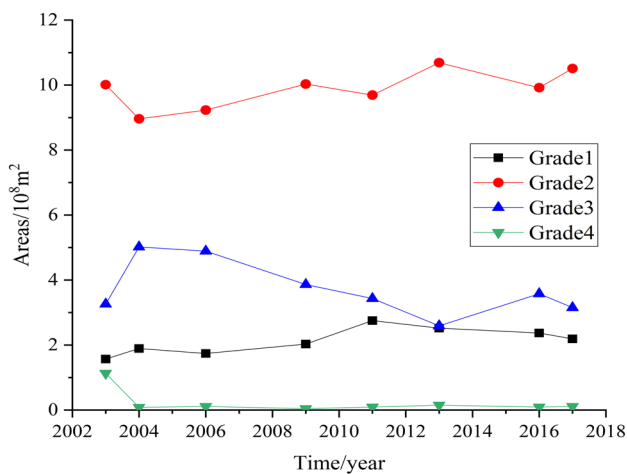


Fig. 8 Changes of grades of surface vegetation coverage in the eastern part of the Eastern Junggar coalfield

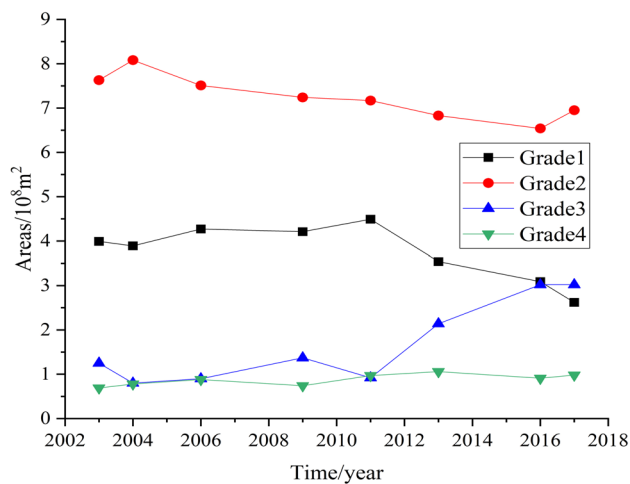


Fig. 9 Change of grades of surface vegetation coverage in the southern part of the Eastern Junggar coalfield

plants pose a potential influence on the glaciers' melting and freezing cycle. Long-term operation of coal mines and coal

power plants in the Eastern Junggar coalfield could have a profound influence on these glaciers.

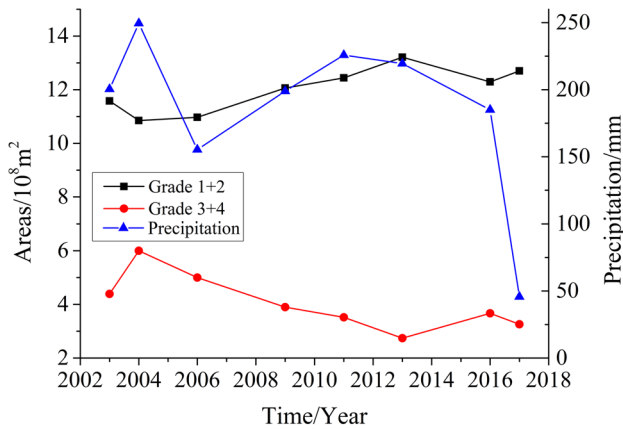


Fig. 10 Relationship between grades of surface vegetation coverage and precipitation in the eastern part of the Eastern Junggar coalfield

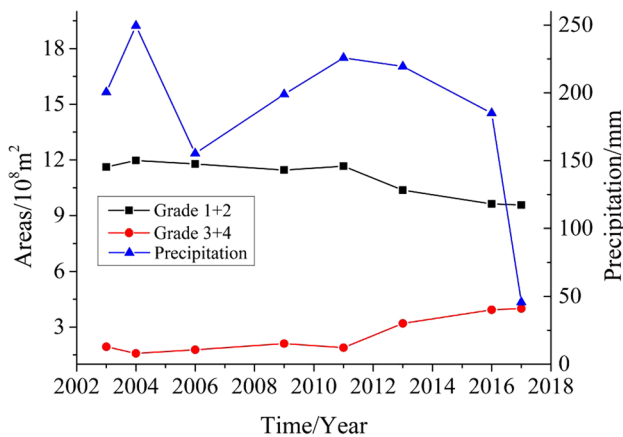


Fig. 11 Relationship between grades of surface vegetation coverage and precipitation in the southern part of the Eastern Junggar coalfield

Numerical simulation of mining damage to ground aquifer

An overlying aquifer is an important rock formation for the storage and transportation of water. This formation

Fig. 12 Surface anomalies in the western part of the Jiangjun-gebi mining area



may also connect to surface and subsurface water systems, which forms a hydraulic relation between them. When the coal beneath the aquifer is mined out, the formation of the aquifers will subside and form fractures along it. Sometimes, these fractures will reach the surface which form a path to connect the surface water and the ground water. Once this situation has occurred, the mining of the coal will certainly cause an impact on regional water distribution.

In this section, the author attempts to investigate the change in the permeability of overlying aquifers using numerical method, which is a key parameter for describing the movement of water within the rocks of aquifers.

According to the data of the lithological column of bore-hole, the hydraulic geology conditions and the overlying rocks' mechanics properties in this region, with the application of similar theory, a physical model was established using the experimental apparatus (3.0 m long and 2.5 m high) by mixing different materials (such as sand, fibre, limestone, and gypsum) in different ratios, see Fig. 13. Using this apparatus, experiments with a large mining height of 7 m were conducted. The mining activities were started from left side to right side along the slice of 600 m length. The mining advance interval was determined as 10 m for the first slice, and 20 m for other consequent slices. From Fig. 13, it can also be observed that the mining-induced damage to overlying aquifers. Based on this physical model, the numerical model also was established (Fig. 14).

It was sure that the slice mining method was used in both models. According to the simulation, reference points 1#, 2#, and 3# were employed to indicate its displacement. Point 1# represents the opening position, point 2# represents the middle position, and point 3# represents the end of mining position.

Based on the results from experiments and simulations, the displacement of reference points 1#, 2#, and 3# was plotted, as shown in Fig. 15.

From Fig. 15, it is clear that the displacements of reference points 1#, 2#, and 3# for both the physical and numerical models show the same trend of change with the advance in mining.

Table 2 Gaseous pollutant emissions from coal power plants in the Eastern Junggar coalfield

Year	Gaseous pollutant emission (tons/year)			
	Smoke dust	SO ₂	NO ₂	Industrial dust
2007	84.7	273.8	820.5	1050
2008	123.08	442.96	1633.53	2301.67
2009	141.19	547.59	1734.86	4148.17
2010	317.23	1196.41	2892.44	4568.17
2011	496.43	1886.17	4284.44	4683.4
2012	836.35	2847.19	6257.1	4931.62
2013	865.23	5940.73	7584.48	5918.68

Mining activities damage the overlying aquifers by affecting the properties of aquifers rocks, such as the stress, porosity, permeability, and others. The permeability of aquifers is an important parameter of describing the capacity of the

fluid transporting through; it is one of the core indicators employed to quantify the change of water flow within aquifers. This change is coupled with coal mining activities. Under certain conditions, this change also leads to a change in surface vegetation due to the change in distribution of surface water affected by mining. Hence, the permeability of the aquifers was selected for investigation in the present study.

In general, the overlying aquifer consists of porous medium and fractures/cracks. For the porous medium, the permeability can be calculated by the following formula:

$$\Phi_{\sigma} = V_{\sigma}/V_1, \quad (3)$$

where Φ_{σ} denotes the porosity of rocks at stress σ with unit of percentage; V_{σ} denotes the volume of porosity at stress σ with unit of m³; V_1 denotes the total volume of the rock matrix of the aquifer with unit of m³.

Table 3 Statistics of solid wastes from coal power plants in the Eastern Junggar coalfield

Power plants	Scale (MW)	Consumed coal (10 ⁴ t/a)	Fly ash (10 ⁴ t/a)	Residues (10 ⁴ t/a)	De-sulphur (10 ⁴ t/a)
Dajing Power Plant, State Grid Energy Ltd.	2×660	316.32	22.55	2.52	5.00
Wucaiwan Power Plant, Sino-Electricity Invest Ltd.	2×660	312.32	24.49	2.73	8.60
Wucaiwan Power Plant, Hua Energy Ltd.	2×660	359.70	12.99	1.45	7.09
Wucaiwan Power Plant4, Sino Coal Energy Ltd.	2×660	252.60	20.60	2.30	8.50
Wucaiwan Power Plant, State Electricity Ltd.	2×660	348.80	24.40	2.72	7.31
Yingema Power Plant	2×660	322.30	18.59	3.30	4.38
Wucaiwan Power Plant, Datang Ltd.	2×660	350.42	12.50	1.40	12.18
Wucaiwan Power Plant, Shendong Branch of Shenhua Group	2×660	318.66	14.91	1.66	12.50
Wucaiwan Power Plant, Tebian Group	2×660	347.60	13.39	1.50	9.00
Zhundong Power Plant, Luan Group	2×660	303.00	30.34	5.37	11.48
Sum	13,200	3231.72	194.76	24.95	86.04

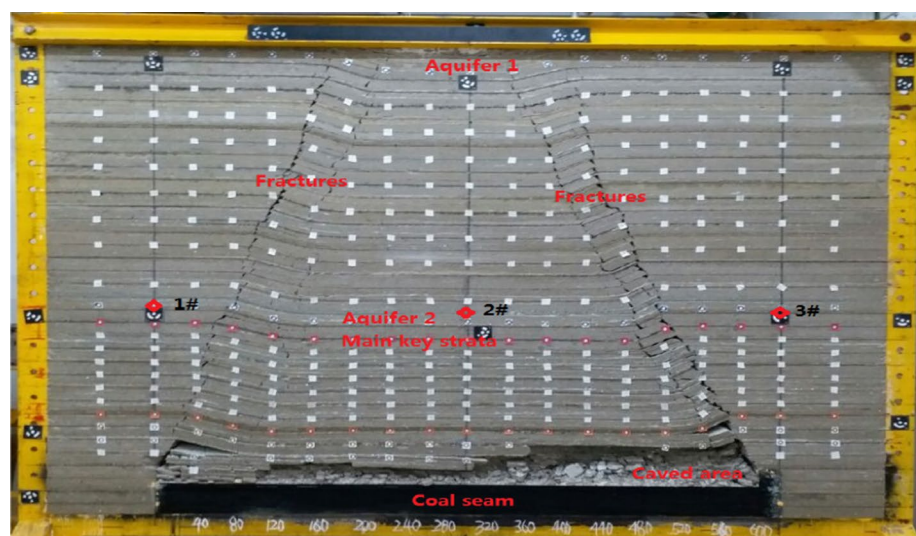
Fig. 13 Physical experiments for slice mining of the super-thick coal seam in Eastern Junggar coalfield

Fig. 14 Numerical model of overlying rocks

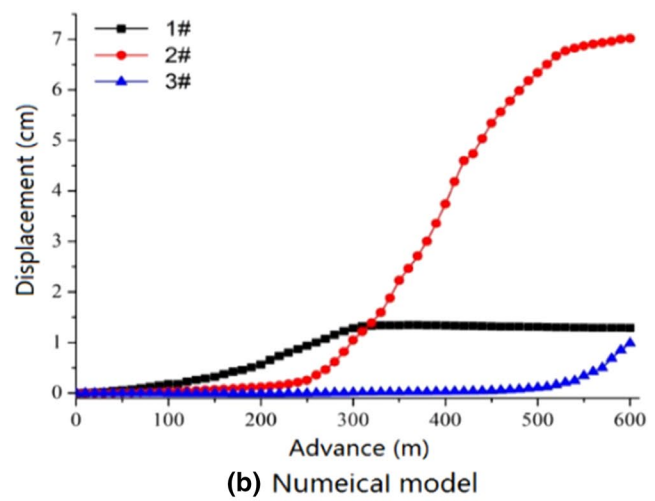
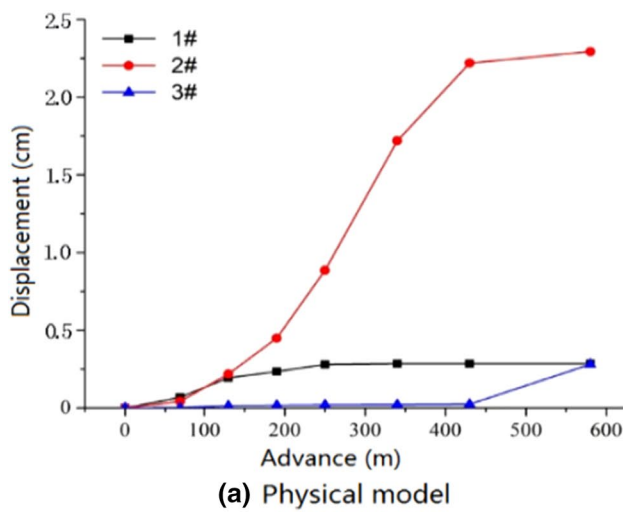
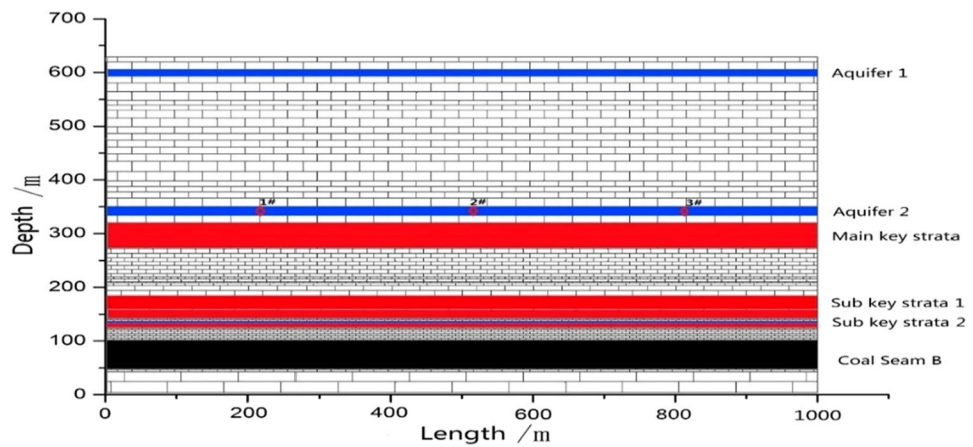


Fig. 15 Displacement of reference points with the advance of mining

According to the Terzaghi theory, the effective stress of saturated rock can be calculated as follows:

$$\sigma' = \sigma - \rho gH, \tag{4}$$

where σ' denotes the effective stress of rocks with unit of Pa; σ denotes the total stress of rocks with unit of Pa; ρ denotes the fluid density with unit of kg/m^3 ; H denotes the potential pressure of fluid with unit of m.

Considering the surrounding condition of less effective stress and the low permeability of depositing rocks, a relationship of the effective stress and the porosity of rock matrix exists as follows:

$$\Phi_{\sigma'} = \Phi_0 \exp(-c\sigma'), \tag{5}$$

where $\Phi_{\sigma'}$ denotes the porosity of rock at effective stress σ' (%); Φ_0 denotes the initial porosity (%); c denotes the matter constant.

For the porous rock matrix, its permeability has a positive relationship with the cubic of the value of porosity, and can be calculated as follows:

$$k_p = k_0 (\Phi_{\sigma'} / \Phi_0)^3, \tag{6}$$

where k_p denotes the permeability of porous rock (m^2); k_0 denotes the initial permeability of rock with (m^2); Φ_0 denotes the initial porosity of rock matrix (%).

For the fracture of the rock matrix, its permeability is influenced by of the effective stress and the width of fractures. The width of the fracture can be calculated as:

$$b_{\sigma} = (\sigma - \rho gH) / E, \tag{7}$$

where b_{σ} denotes the width of the fracture at stress σ (Pa); E denotes the plastic module.

For a rock matrix with a single fracture, its permeability can be calculated by the following formula:

$$k_f = \beta \cdot \rho \cdot g \cdot b_\sigma / 12\mu C, \quad (8)$$

where k_f denotes the permeability of the rock fracture (m^2); β denotes the ratio of the connected area of fractures to the total area of fractures; μ denotes the inherent coefficient of movement of fluid with unit of $\text{N}\cdot\text{s}/\text{m}^2$; C denotes the roughness correction coefficient of the fracture.

The required parameters and their values, which were used to simulate the change in stress in the rocks using UDEC (Itasca Consulting Group, USA), are listed in Table 4.

Based on the numerical model of mining (see Fig. 14), a simulation was done to quantify the change in permeability of the reference points in the aquifer based on Eqs. (5)–(8). Figure 16a shows the changes in the porous rock matrix permeability of reference points associated with the mining of the first slice. Figure 16b shows the changes in the fracture

permeability of reference points associated with the mining of the first slice.

From Fig. 16a, it can be observed that the porous rock matrix permeability of the reference point 1# increased with the advance in mining from opening to 100 m, and then decreased from 100 to 175 m, and then remained stable from 175 to 300 m. After 300 m, the permeability increased again until 350 m, and then decreased until the end position of mining. Regarding point 2#, its porous rock matrix permeability decreased with the advance in mining face from the opening to 275 m, then increased until 450 m, and then decreased until the end of mining. Regarding the point 3#, its porous rock matrix permeability stays stable with the mining of coal from the opening to 250 m, and then slowly decreased until the position of 400 m. Furthermore, after a small increase until 500 m, the permeability reduced rapidly until 575 m. During the mining of the last 25 m of the coal seam, the permeability increased rapidly. The permeability of the point 2# shows a sharp fluctuation during the entire process in the mining of the first slice.

From Fig. 16b, it is obvious that the permeability of the fractures of the point 1# decreased with the advance of mining from the opening to 100 m, then increased until 200 m, and then decreased again till 350 m. Thereafter, the permeability increased slowly until the end of mining. Regarding point 2#, its fracture permeability increased from the opening to 270 m and then decreased sharply until 350 m. After that, this permeability remained stable till the mining position of 550 m; it increased again until the end of mining. Regarding point 3#, its fracture permeability remained stable from the position of opening to the position of 275 m and then increased until the mining position of 325 m. After that, this permeability remained almost stable till 500 m. During the final 100 mining length of working face, this permeability increased sharply from the position of 500 m

Table 4 Parameters for simulation and calculation of permeability

Parameters	Values/unit
Potential pressure of fluid	311 m
Gravity constant, g	10 g/m^3
Plastic module, E	1.45 GPa
Matter constant, c	$0.5 \times 10^{-3} \text{ MPa}^{-1}$
Initiate porosity of rock matrix, Φ_0	10%
Initiate permeability of rock, k_0	$4.55 \times 10^{-10} \text{ m}^2$
Fluid density ρ	1000 kg/m^3
Inherent coefficient of movement of fluid, μ denotes	1.01 Pa s
Ratio of the connected area of fractures to the total area of fractures, β	1
Fractures' roughness correction coefficient, C	1

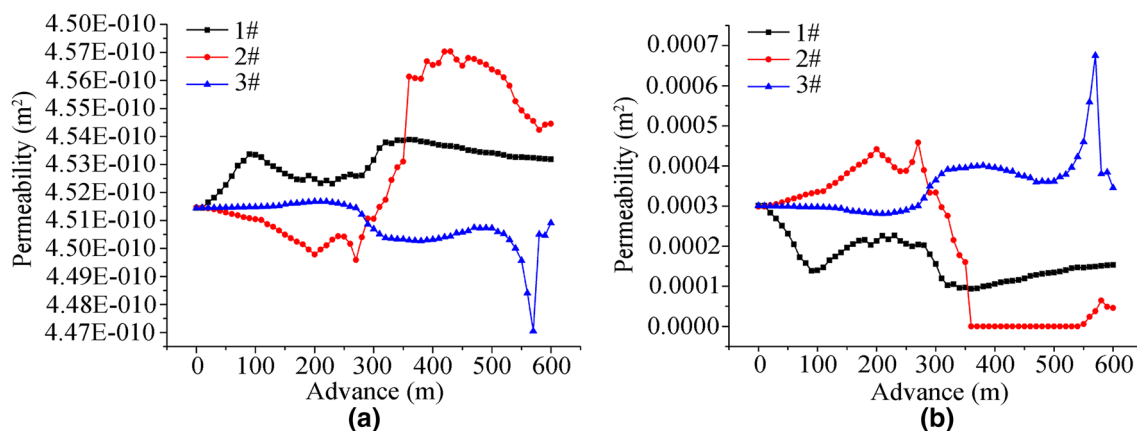


Fig. 16 Changes in permeability of the porous (a) and fracture (b) of overlying rocks with the advance in mining of the first slice

to the position of 550 m and then decreased till the end of the mining.

From the above analysis of the permeabilities of the porous rock matrix and the fracture of rock, it is obvious that both these two types of permeabilities vary with the mining activities, which leads to change in groundwater distribution in the mining area (including affected areas of the aquifer). Generally, a funnel shape of ground water is formed due to the mining of a coal seam. Considering the large area of the Eastern Junggar coalfield, formed funnels vary with the mining activities in this region, such as the change in range of funnels, the connection of different formed funnels to form a larger funnel, and similar. Due to the deposition of the super-thick coal seam, the large range of coal deposition in this region, and the intensity of mining activities, it is certain that coal mining will redistribute the surface and subsurface water system which has an important impact on surface vegetation in this region. It is also one reason that the author chose to focus on this issue. However, this topic merits further investigation.

To investigate the further changes associated with mining of the sub slices, the consequent simulations were made according to the procedures of mining from subslice 1 to subslice 8. Using Eqs. (5)–(8), the changes in permeability of each point (including those of porous rock matrix and fractures) were calculated and plotted (Fig. 17a, b).

From Fig. 17a, it is clear that the porous rock matrix permeability of point 1# and point 3# generally has the same trend of change with the mining of subslices. That is, the permeability increased associated with the consequent mining of subslice 1–subslices 8. Meanwhile, the permeability of point 2# showed a fluctuation during the process of the mining of these subslices.

From Fig. 17b, it was observed that the fracture permeability of point 1# decreased with the mining of the subslice

1 and subslice 2, and then stays stable till the mining of subslice 8. The permeability of point 3# decreased in general with the mining of subslices except the mining of subslice 1 and subslice 4. The permeability of point 2# also shows a fluctuation during the process of mining of different subslices and peaks at the mining of subslice 4.

In general, from Figs. 16 and 17, it is obvious that different areas show different permeability during the entire process of mining the coal seam. With reference to Fig. 3b, these distinguished differences of permeability will lead the characteristics of groundwater transportation and distribution which is very important to the local environment.

Besides the damage to ground water induced by mining, the shallow aquifer also can be damaged by underground mining and open-pit mining. Generally, the overlying rocks will cave in after coal were mined out due to gravity. When the caved area reaches the point where the vertical fracturing area goes to the aquifers, the water contained in the aquifers will flow along fractures, which will cause redistribution of water contained in aquifer. Sometimes, this redistribution of ground water also causes redistribution of the regional surface and subsurface water system. This phenomenon is very important for the growth and distribution of surface vegetation.

From the above analysis, it can be concluded that underground mining leads to damage of ground and shallow aquifers in this region, and the open-pit mining leads to damage of the shallow aquifer. Both types of damage lead to redistribution of the water system in this region which leads to consequent impact on the local environment.

As a case to illustrate the impact of coal mining activities on ground water, the groundwater level of Qitai oasis was investigated by the author. The area for this investigation was in the northern part of the Qitai oasis which surrounds the southern part of the Eastern Junggar coalfield.

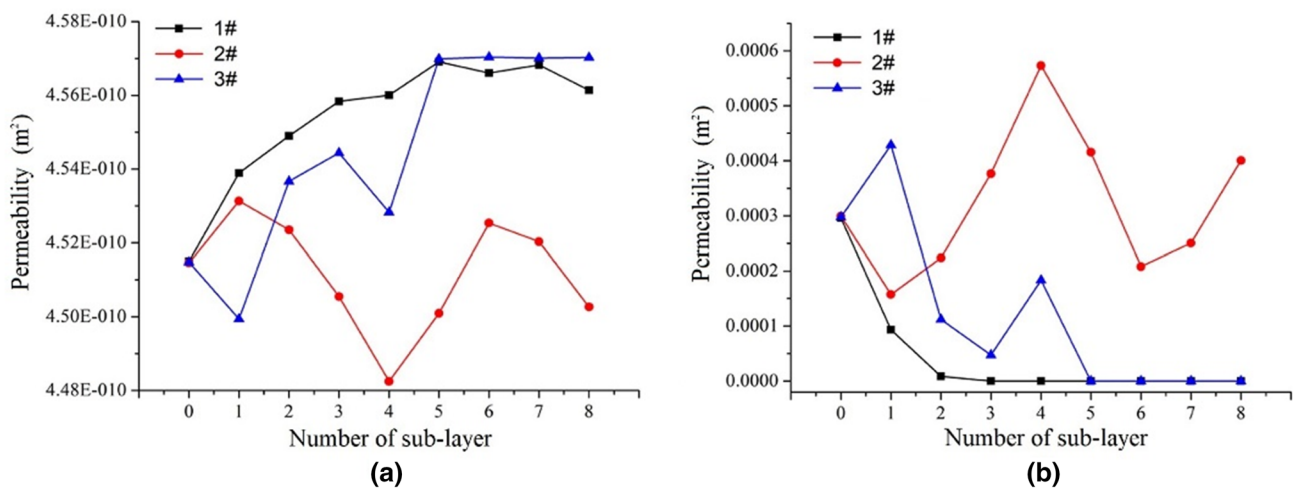


Fig. 17 Change in permeability of porous rock matrix (a) and fracture (b) with the mining of subslices

Fig. 18 Change in groundwater levels in the Qitai oasis from 1983 to 2013

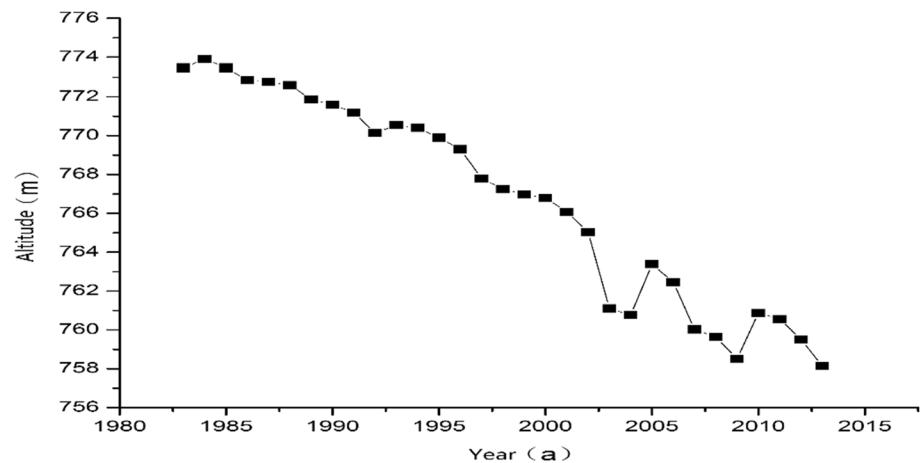
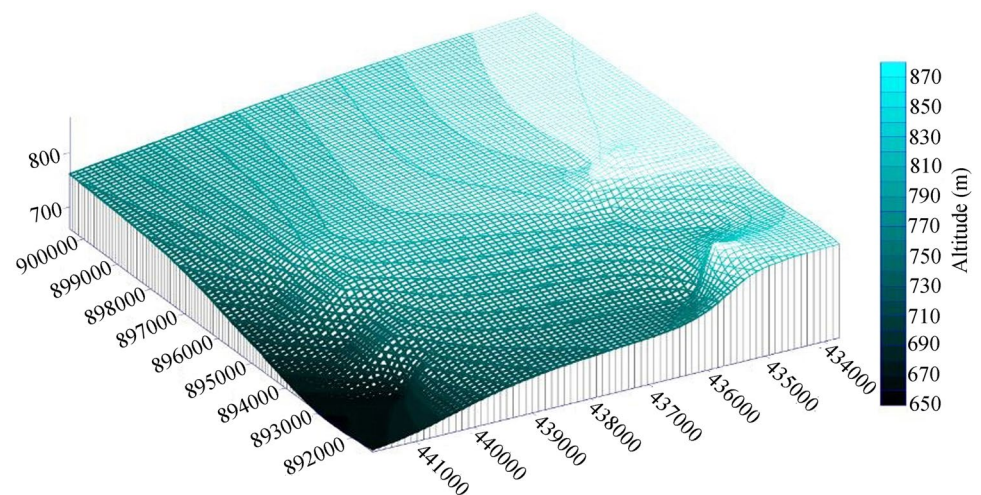


Fig. 19 Distribution of groundwater level in part of the Qitai oasis in 2013



From surveying more than 30 water wells from 1983 to 2013 in this area, the water-level data were collected and compiled to plot the change in groundwater level, see Fig. 18. The distribution of the groundwater level in 2013 in this area is also plotted as Fig. 19.

From Fig. 18, the groundwater level decreased from +774 m in 1983 to +758 m in 2013. Twenty-six meters in water-level difference occurred in past 30 years. From Fig. 19, an obvious water funnel was formed in this area due to the decrease in water level in the past decades.

Conclusions

This study attempts to study the potential impacts of the mining of the super-thick coal seam on local environment in arid eastern Junggar region of China. Some conclusions were obtained as follows:

1. The low surface vegetation coverage (grade 1 plus grade 2) in the southern part of this region decreased from $11.62 \times 10^8 \text{ m}^2$ in 2003 to $9.57 \times 10^8 \text{ m}^2$ in 2017, while it increased from $11.58 \times 10^8 \text{ m}^2$ in 2003 to $12.70 \times 10^8 \text{ m}^2$ in 2017 in the eastern part. The high surface vegetation coverage (grade 3 plus grade 4) in the southern part increased from $1.94 \times 10^8 \text{ m}^2$ in 2003 to $4.00 \times 10^8 \text{ m}^2$ in 2017, while it decreased from $4.39 \times 10^8 \text{ m}^2$ to $3.26 \times 10^8 \text{ m}^2$ in the eastern part. And it is clear that the changes of surface vegetation coverage in the east and south parts of this region have less relationship with annual precipitations, which indicates that the mining activities are probably the major reason for that.
2. The pit coal power plants are also a major source of pollutants. There are estimated 865.23 tons of smoke particles, 5940.73 tons of SO_2 , and 7584.48 tons of NO_2 released from these plants in 2013, which are 9.73 times, 21.69 times, and 9.24 times than that of corresponding pollutants in 2007. These pollutants not only have an

impact on the local environment, but also pose a potential risk of contamination to glaciers in remote mountainous areas.

3. Physical and numerical simulation of the damage of mining activities to aquifers shows that the permeability of the reference points of overlying aquifers varies associated with mining. The porous rock matrix permeability shows a negative relationship with fluctuation during mining, while the fracture permeability shows a positive one. Due to the super-thickness of the coal seam and the large area of coal deposition in this region, the damage and disturbance induced by mining activities to local environment (especially to the surface and subsurface water system) need to be emphasized.
4. A case study of the change of groundwater level in Qitai oasis also illustrates the potential risk of coal mining activities in the Eastern Junggar coalfield to surrounding oasis environment system. This risk needs to be evaluated comprehensively.

Acknowledgements This study was supported by the National Natural Science Foundation of China with grant no. 51374182 and the Department of Science and Technology of Xinjiang Province Government of China with grant no. 2018E01011.

References

- Bahrami S, Ardejani FD, Baafi E (2016) Application of artificial neural network coupled with genetic algorithm and simulated annealing to solve groundwater inflow problem to an advancing open pit mine. *J Hydrol* 536(2016):471–484
- Daozhong C, Qingli Z, Jie W, Xiaozhi Z (2011) Comparative analysis of ecological rucksack between open-pit and underground coal mine. *Energy Procedia* 5(2011):1116–1120
- da Silvaa MG, Muniz ARC, Hoffmann R, Lisbôa ACL (2018) Impact of greenhouse gases on surface coal mining in Brazil. *J Clean Prod* 193(2018):206–216
- Espitia-Pérez L, Arteaga-Pertuz M, Soto JS, Espitia-Pérez P, Salcedo-Arteaga S, Pastor-Sierra K, Galeano-Páez C, Brango H, da Silva J, Henriques JAP (2018) Geospatial analysis of residential proximity to open-pit coal mining areas in relation to micronuclei frequency, particulate matter concentration, and elemental enrichment factors. *Chemosphere* 206(2018):203–216
- Huang L, Zhang P, Hu Y, Zhao Y (2015) Vegetation succession and soil infiltration characteristics under different aged refuse dumps at the Heidaigou opencast coal mine. *Glob Ecol Conserv* 4(2015):255–263
- Huang L, Zhang P, Hu Y, Zhao Y (2016) Vegetation and soil restoration in refuse dumps from open pit coalmines. *Ecol Eng* 94(2016):638–646
- Huertas JI, Huertas ME, Izquierdo S, González ED (2012) Air quality impact assessment of multiple open pit coal mines in northern Colombia. *J Environ Manag* 93(2012):121–129
- Huisamen A, Wolkersdorfer C (2016) Modelling the hydrogeochemical evolution of mine water in a decommissioned opencast coal mine. *Int J Coal Geol* 164(2016):2–12
- Hussain R, Wei C, Luo K (2019) Hydrogeochemical characteristics, source identification and health risks of surface water and groundwater in mining and non-mining areas of Handan, China. *Environ Earth Sci* 78(2019):402–422
- Jie J (2015) Study on simulation of atmospheric pollution in the Economic Technological Development Zone of Eastern Junggar Basin (Thesis). Xinjiang Agriculture University, Urumqi, China
- Kumari S, Maiti SK (2019) Reclamation of coalmine spoils with topsoil, grass, and legume: a case study from India. *Environ Earth Sci* 78(14):429. <https://doi.org/10.1007/s12665-019-8446-2>
- Liu XY, Wei ZA, Bai ZK (2016) Vegetation coverage change and stability in large open-pit coal mine dumps in China during 1990–2015. *Ecol Eng* 95(2016):447–451
- Reisen F, Gillett R, Choi J, Fisher G, Torre P (2017) Characteristics of an open-cut coal mine fire pollution event. *Atmos Environ* 151(2017):140–151
- Yongjun Y, Erskine PD, Shaoliang Z, Yunjia W, Zhengfu B, Shaogang L (2018) Effects of underground mining on vegetation and environmental patterns in a semi-arid watershed with implications for resilience management. *Environ Earth Sci* 77(2018):605–616
- Zhao L, Ren T, Wang N (2017) Groundwater impact of open cut coal mine and an assessment methodology: a case study in NSW. *Int J Min Sci Technol* 27(2017):861–866

Publisher's Note Springer Nature remains neutral with regard to jurisdictional claims in published maps and institutional affiliations.